1300-nm Strained Quantum Well Lasers For Fiber-Optic Communications

William S. Ring
Simon J. Wrathall
Adrian J. Taylor

This paper describes new uncooled strained quantum well lasers for SONET/SDH systems. New Fabry-Perot lasers for short-haul and intermediate link applications are extremely reliable, have high ex-facet power, and have record low threshold currents, making lower packaging costs possible. Uncooled distributed feedback lasers for the long-haul market at 622 Mbits/s and 2.488 Gbits/s are discussed. These operate from −40°C to +85°C with extremely good threshold and power characteristics.

In recent years there has been increased emphasis on cost and performance issues for telecommunications lasers. The drive to push fiber to the curb (FTTC) and fiber to the home (FTTH) can only be fully realized when inexpensive laser transmitter modules become available.

The drive for lower cost has forced the move to uncooled semiconductor lasers, which require high output powers and low threshold currents over the temperature range of −40°C to +85°C, combined with inexpensive packaging technology. The type of laser used depends primarily on the link length and operating speed. The Synchronous Digital Hierarchy (SDH/SONET/ATM) standards pertaining to the use of either multimode or single-mode lasers specify the basic requirements for spectral purity and operating wavelength range appropriate to the fiber characteristics. They also dictate whether a multimode, Fabry-Perot laser or a single-mode, distributed feedback (DFB) laser is used in the system.[1] For most short-haul and intermediate link length applications, the STM-1 (155 Mbits/s) and STM-4 (622 Mbits/s) standards dictate that a Fabry-Perot laser should be suitable. For long-haul applications a distributed feedback laser is recommended for wavelength stability and dispersion. As systems move to higher speeds, such as STM-16 (2.5 Gbits/s) the emphasis moves to distributed feedback lasers, even for shorter link lengths.

For the STM-1 and STM-4 short-haul and intermediate links, 1300-nm Fabry-Perot lasers are the main devices employed. For operation without a thermoelectric cooler there are difficulties in designing a laser that is temperature insensitive and has high output power. It has been known for some time that long-wavelength telecommunication lasers suffer from an inherent temperature sensitivity problem that is not observed in short-wavelength, GaAs-based devices. This is believed to result from the small bandgap and the associated nonradiative and absorptive processes of Auger recombination and intervalence band absorption, which then become significant at longer wavelengths.

Fabry-Perot 1300-nm Strained Quantum Well Lasers

It was predicted theoretically in 1986 that introducing strained layers in the active region of long-wavelength lasers should improve the temperature performance.[2, 3] The physics behind this is that the strain introduced in the crystal lattice splits the degeneracy of the two valence bands in the semiconductor, enhancing either TE (transverse electric) polarization optical gain or TM (transverse magnetic) polarization optical gain (see **Figure 1**). The strain can be accommodated elastically if the total thickness of the strained layer is less than the critical thickness of the material system. Critical thickness is the point at which the elastic energy in the layer is equal to the energy required to introduce dislocations into the crystal lattice. The value of the critical thickness was originally calculated by Mathews and Blakeslee[4] and is equivalent to a strain-thickness product of approximately 10 nm% for InGaAsP/InP (e.g., a 10-nm thickness with 1% strain). For practical device purposes, only thin layers, that is, strained quantum well devices, can realistically be grown.

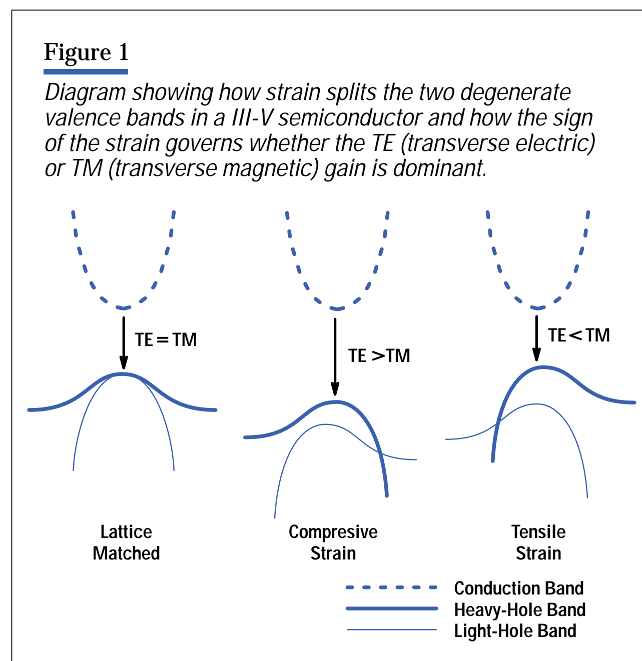

Figure 1

Diagram showing how strain splits the two degenerate valence bands in a III-V semiconductor and how the sign of the strain governs whether the TE (transverse electric) or TM (transverse magnetic) gain is dominant.

The first realization of strained quantum well devices occurred for 1550-nm strained quantum well lasers in 1989 and 1990 with the demonstration of increased ex-facet power (power out of the laser chip into a broad-area detector) and reduced threshold current. A high characteristic temperature (T_o) of 90K was reported.[5] Initial effort mainly concentrated on 1550-nm devices for long-haul links to improve the power budget. Meanwhile, work on 1300-nm quantum well devices has highlighted another factor that leads to increased temperature sensitivity: loss of carriers out of the quantum well.[6,7]

Design Issues

The most common material system used to grow 1300-nm and 1550-nm long-wavelength lasers is the InGaAsP/InP system. This material system suffers from the fact that the ratio of the conduction band to the direct bandgap is 0.4, compared to an estimated 0.6 to 0.85 for GaAs-based systems. For 1300-nm quantum well lasers this leads to an energy difference between the electron confined state and the barrier material on the order of 1 to 2 k_bT or 25 to 50 meV at room temperature. This can lead to a significant excitation of carriers out of the quantum well or a large carrier density in the barrier material at elevated temperatures. A large carrier density in the barrier material degrades the performance of the laser, causing increased temperature sensitivity and reduced ex-facet power.

An alternative material system is the InGaAlAs/InP system, in which the ratio of the conduction band to the direct bandgap is 0.7. This gives increased electron confinement. The electron confined state energy can then be designed to be 4 to 5 k_bT or 100 to 150 meV at room temperature,[8] significantly larger than the InGaAsP system. Unfortunately, because of the aluminum content and associated reliability issues, only ***ridge laser structures*** are presently fabricated using this material system. To achieve low threshold currents, ***buried heterostructure lasers***, which have better electrical and optical confinement, are preferred.

We have investigated 1300-nm strained InGaAsP/InP active regions to try to optimize the device performance for low threshold current and high ex-facet power from −40°C to +85°C. The following section outlines the main results from our experiments, which led to the development of a highly successful 1300-nm quantum well laser.

Optimization of Confined State and Barrier Energy

The energy difference between the electron confined state in the quantum well and the barrier layer can be calculated using a crystal energy band modeling method[9] (model solid method) combined with a k.p effective mass one-dimensional square well potential model. The k.p method is a band structure modeling technique by which the effective mass of the electrons and holes is calculated from the energy gaps of the semiconductor.

The model solid method calculates the band edge energies relative to the vacuum level using a density functional mathematical method. These can then be used to calculate the conduction band and valence band energy offsets, that is, the depth of the quantum wells. These, combined with the effective mass and its energy dependence from k.p theory, are used to find the positions of the energy states in the quantum well.

To optimize the energy difference, the well, barrier composition, and well width are varied. To illustrate the enhancement that can be achieved using a strained quantum well compared to a lattice matched quantum well structure, we have plotted in **Figure 2** the energy difference as a function of well width. For the equivalent emission wavelength of 1300 nm there is an improvement in energy difference for the strained layer structure. This, coupled with (1) the smaller carrier density in the quantum well due to increased differential gain and (2) the polarization discrimination of the strain layers, improves the device characteristics.

Fabrication

To understand the design limits for the Fabry-Perot laser device, we grew several wafers with the same active-region strain, but different numbers of quantum wells and different guide layer (separate confinement heterostructure) thickness. The devices were grown using atmospheric-pressure metal organic chemical vapor deposition (MOCVD) in a horizontally configured Thomas Swan reactor. The strain in the quantum wells was fixed at 0.8% and the well width was 6 nm. All wafers were fabricated into our standard buried heterostructure, which uses a p-n-p-n current blocking structure to confine the current to the active region.

Internal Loss

The external ex-facet efficiency is related to the internal optical absorption loss in the cavity by the following expression, originally given by Biard.[10]

$$\frac{1}{\eta_d} = \frac{1}{\eta_i} + \frac{\alpha_i L}{\eta_i \ln(1/R)}, \qquad (1)$$

where L is the cavity length, R is the facet reflectivity, α_i is the internal absorption loss, η_i is the internal quantum efficiency, and η_d is the external differential quantum efficiency. Using equation 1 and plotting the inverse of the differential efficiency against the cavity length we can obtain a value for the internal loss of the laser cavity.

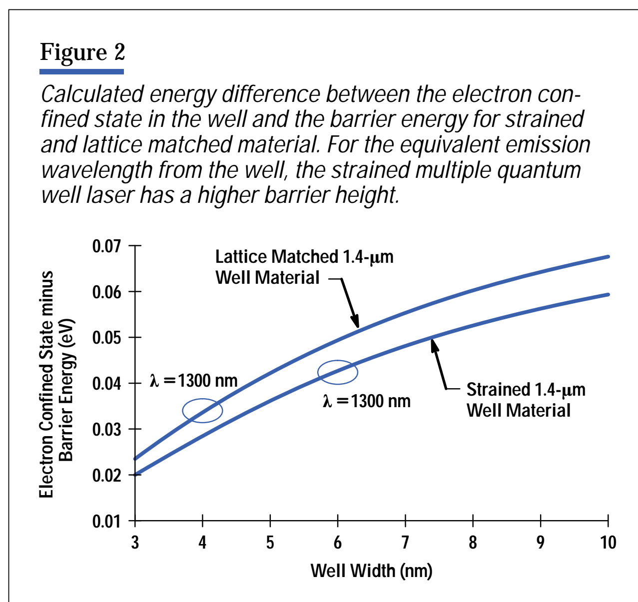

Figure 2

Calculated energy difference between the electron confined state in the well and the barrier energy for strained and lattice matched material. For the equivalent emission wavelength from the well, the strained multiple quantum well laser has a higher barrier height.

In a quantum well laser, when there is no intervalence-band absorption, the internal loss per quantum well should be linear with the number of wells, since the internal losses do not depend on carrier density. We plotted the calculated internal loss for devices with different numbers of wells and found a linear dependence (see **Figure 3**). The lowest loss obtained was 4.5 cm^{-1} for four quantum wells. This equates to an ex-facet slope efficiency of 0.42 mW/mA for a 350-µm-long chip, with $\eta_i = 0.98$. Higher output powers can be obtained if a high-reflectivity coating is then applied to one of the facets, because the low internal absorption loss allows more photons to travel in one round trip in the cavity and escape out of the uncoated facet. Typically the uncoated cleaved facet efficiency can be 0.6 mW/mA for a cleaved and high-reflectivity coated device.

Gain-Current Curves at 25°C

A useful tool for understanding the performance of the laser is a gain-current curve. This can be obtained experimentally by combining the measured internal loss with the variation of the threshold current density per unit length. Normally the gain of a semiconductor laser can be approximated by the following logarithmic expression, which takes into account the saturation of the gain spectrum at high current densities:

$$G = G_o \left[\ln\left(\frac{\eta_i J_{thr}}{J_{tr}} \right) + 1 \right], \qquad (2)$$

where G is the modal gain and is related to the material gain g by the optical confinement factor Γ (the overlap of the optical field with the active material), that is, $G = \Gamma g$, η_i is the internal quantum efficiency, J_{thr} is the threshold current density in A/cm^2, J_{tr} is the transparency current density in A/cm^2, and G_o is the modal gain coefficient. If we rearrange equation 2 and plot $\ln(J_{thr})$ versus the inverse of the length, the slope of the graph gives the modal gain coefficient G_o and

Figure 3

Measured variation in the internal absorption loss for 0.8% strained multiple quantum well lasers as a function of the number of wells at 25°C. This demonstrates the negligible effect of intervalence band absorption in 1300-nm strained material.

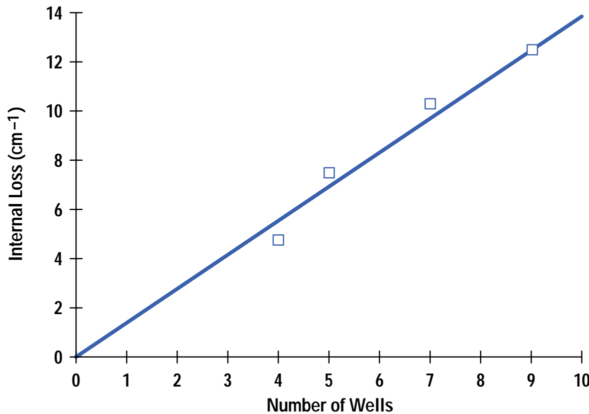

Figure 4

Measured gain-current curves for 9-, 7-, 5-, and 4-well active regions at room temperature. The smaller the number of wells the flatter the gain curve at higher current density.

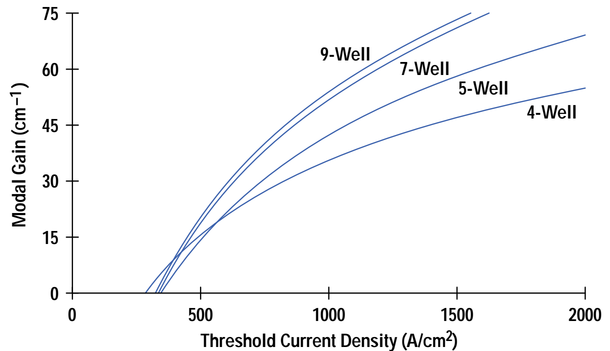

the intercept is related to the transparency current density J_{tr}. The modal gain varies with the number of quantum wells in the structure (see **Figure 4**). The smaller the number of wells the faster the gain rolls off with increasing current density. For 9-well and 7-well material the gain-current curves are very similar at 25°C, but as we will see later from the temperature dependence of the threshold current, a difference becomes apparent, especially when trying to optimize for good 85°C characteristics.

Threshold Current between 25°C and 85°C

The relationship between threshold current and temperature for semiconductor lasers is commonly characterized by an exponential function, which is used to associate a characteristic temperature T_o with the device structure.[11] The expression is:

$$J_{th}(T_2) = J_{th}(T_1)\exp(\Delta T/T_o), \qquad (3)$$

where J_{th} is the threshold current or threshold current density and $\Delta T = T_2 - T_1$ is the temperature difference. This expression is essentially valid only above 250K, when the threshold current begins to increase rapidly with temperature.

The target threshold current for the product was a maximum of 30 mA at 85°C. Different active region structures were characterized over temperature and a strong correlation of the threshold current with the number of quantum wells at elevated temperatures was observed (see **Figure 5**). For 5-well structures the threshold current increased from 5 mA to 44 mA for 350-µm-long devices ($T_o \approx 28K$). Meanwhile, 9-well devices showed increases from 5 mA to only 18 mA ($T_o \approx 48K$) over the same temperature range. To understand the role played by the optical guide layer thickness on either side of the quantum wells, we compared 5-well and 7-well material (see **Figure 6**). It was very noticeable that the threshold current increased more dramatically for 5-well material than for the 7-well material for the same guide layer. This showed us that the current density, or equivalently, the carrier density per quantum well, was the dominant mechanism affecting the temperature sensitivity. This indicated that the excitation out of the well material into the barrier layer was a primary loss mechanism at elevated temperatures for InGaAsP-based lasers at 1300-nm wavelength. To further understand the significance of this effect we compared the external differential efficiency between 25°C and 85°C.

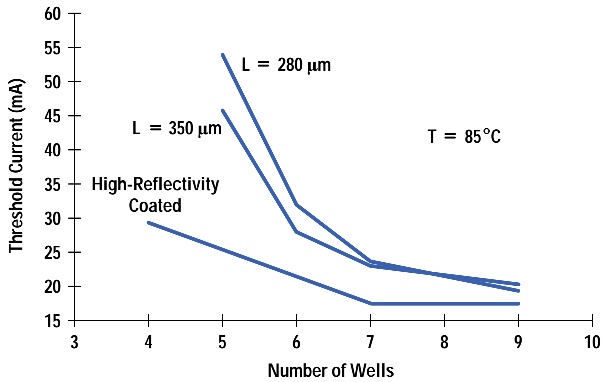

Figure 5

Plotted is the trend in threshold current for 280-μm, 350-μm, and cleaved high-reflection coated devices for different numbers of quantum wells in the active region at 85°C. The smaller the number of wells the worse the temperature performance due to increased escape from the quantum wells.

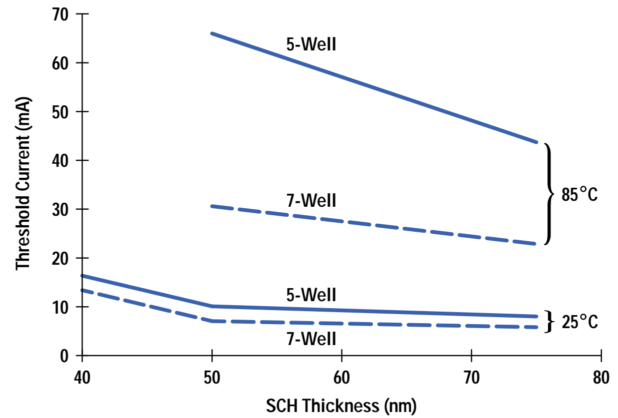

Figure 6

Temperature performance of 5-well and 7-well lasers at 25°C and 85°C as a function of waveguide (separate confinement heterostructure, SCH) thickness. This demonstrates that the number of quantum wells dominates and hence carrier density per well has a more dominant effect than the waveguide width.

Differential Efficiency between 25°C and 85°C

The change in the external differential efficiency is characterized using equation 1. The change in internal loss and internal quantum efficiency can be used as a tool to understand the dominant temperature dependent loss mechanism. When we measured the slope efficiency for the different number of wells and compared the ratio of the 85°C slope efficiency divided by the 25°C slope efficiency, a definite trend became apparent. As the device becomes shorter, the mirror loss of the device increases. When the slope efficiency ratio is plotted as a function of mirror loss (See **Figure 7**), it is evident

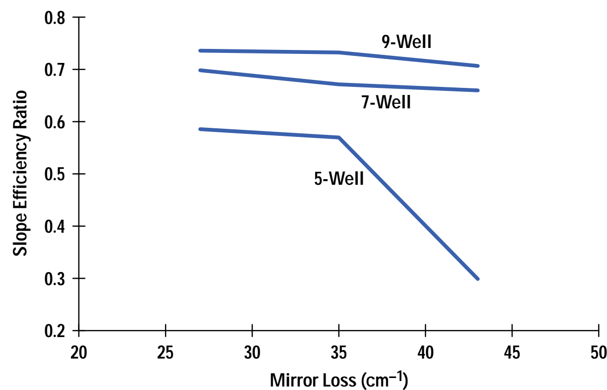

Figure 7

The ratio of the slope efficiency between 85°C and 25°C for 9-, 7-, and 5-well devices is plotted as a function of mirror loss. The main observation is the breakpoint observed for the 5-well device, indicating that the internal quantum efficiency has passed a critical point.

that 9-well and 7-well devices show a linear dependence, which is expected because the internal loss or quantum efficiency did not vary. For the 5-well device a breakpoint is observed, which is consistent with either a rapid increase in internal loss or a rapid degradation in the internal quantum efficiency. In a laser above threshold it is assumed that the internal efficiency is equal to 1, but in the method of Biard,[10] η_i is not equal to 1 because it contains contributions of leakage current, excitation out of the quantum well, and other effects. The evidence suggests that at a critical carrier density, excitation out of the well dominates the laser threshold current and the slope efficiency. Further evidence to support this was found when we constructed a gain-current curve for 7-well devices at both temperatures (see **Figure 8**). The internal absorption loss was found to increase only from 10.3 cm^{-1} to 11.2 cm^{-1}, but η_i decreased from 0.98 to 0.65, showing a marked reduction in electrical-to-optical conversion efficiency.

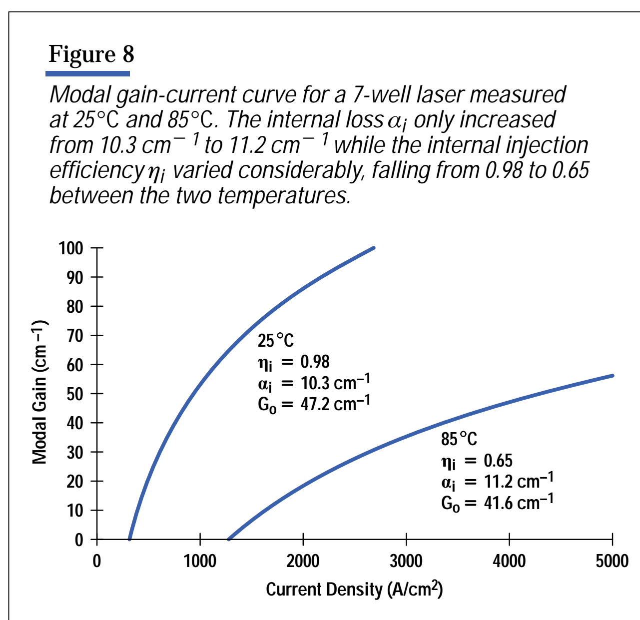

Figure 8

Modal gain-current curve for a 7-well laser measured at 25°C and 85°C. The internal loss α_i only increased from 10.3 cm^{-1} to 11.2 cm^{-1} while the internal injection efficiency η_i varied considerably, falling from 0.98 to 0.65 between the two temperatures.

Reliability

The reliability requirement for telecommunications products is a field lifetime of approximately 25 years.[10] To validate whether the active region design is suitable, an accelerated aging test is performed and predictions for the median and lower tenth percentile lifetimes are calculated. The standard testing regime is to hold the device at 85°C and monitor the change in threshold current with the device driven approximately at rated power.

As initially pointed out, the introduction of strain in the active region of the device can be accommodated elastically only if the total thickness is less than the critical thickness for the material. Dislocation-free material is ideal for a laser device, but typically a defect density of less than $10^4/cm^2$ is sufficient for operation. For a strained multiple quantum well stack it has been shown that a factor of 4 to 6 times the critical thickness can be accommodated before dislocation formation is so severe as to degrade the device performance. A rule of thumb is a maximum critical thickness of 4×10 nm% for a strained multiple quantum well stack.

Dislocation formation in the active region can lead to hot spots and leakage current paths that degrade the device performance over its life. For 9-well devices the estimated strain-thickness product is $9 \times 0.8 \times 6$ nm or 43 nm%, which is over the maximum limit. The 7-well structure is 33 nm% and under. Strain compensation can be introduced by having the opposite mismatch in the guide layers. This is not equivalent to growth of zero-net-strain structures, but can partially compensate the overall strain-thickness product. Both 9-well and 7-well wafers were life tested for 5000 hours and

exhibited linear degradation rates less than 0.75% per 1000 hours (see **Figure 9**). Median lifetimes were predicted assuming a power-law dependence at 85°C. The median life for 7-well lasers was estimated at 2.6×10^5 hr (the failure criterion is median life $< 40,000$ hr at 85°C). The 25°C median life can be calculated, assuming an activation energy of 0.6 eV to convert the accelerated test to its room temperature value. The estimated median life is 1.9×10^7 hr or 2100 years, which is suitable for all telecommunications system applications.

Figure 9

Accelerated aging test at 85°C for 9-well and 7-well devices. The line indicates a degradation rate of 0.75% per khr. Both types of device show very good reliability, with predicted lives of 2.6×10^5 hr at 85°C.

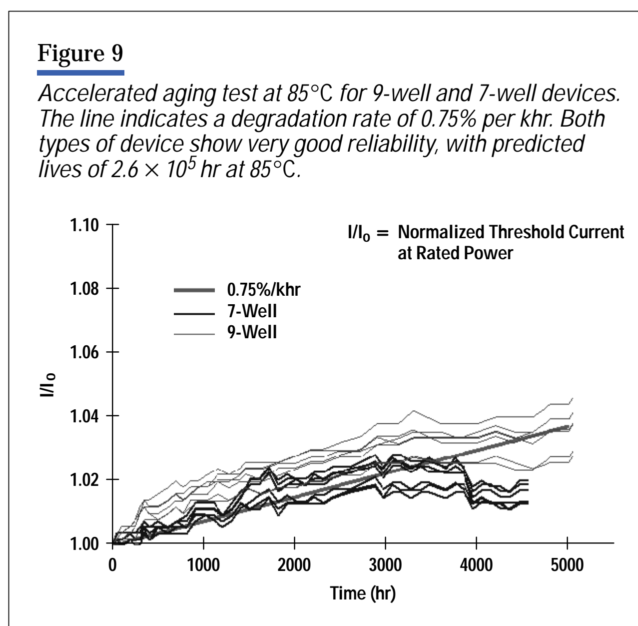

Uncoated 5-well laser devices were also life tested at 85°C, but because of their extremely poor temperature performance, they exhibited large changes in threshold current within the first 600 hours. The typical increase in threshold was approximately 10%. This was unacceptable from both a threshold current and a reliability standpoint and the design was rejected on that basis.

Fabry-Perot Laser Device Conclusions

The main conclusions from the chip investigation above show that the dominant factor affecting the high temperature operation of the 1300-nm InGaAsP/InP buried heterostructure laser is the carrier density per quantum well. To achieve good reliability, high ex-facet power, and low threshold currents, an optimized design of a 7-well device was chosen. The number of quantum wells dominated over the guide layer thickness, allowing us to achieve a nearly circular far field of 27° by 23° by modifying the guide layer thickness at some cost in temperature performance (see **Figure 10**). This approach has been beneficial from a manufacturing and packaging viewpoint. The existing coaxial laser package has recently been superseded by a new welded version that incorporates a ball lens, offering a significant cost reduction compared to the previous package. The lower internal loss and high ex-facet power achieved with a cleaved high-reflectivity coated chip makes it possible to achieve 2 mW out of the fiber without the use of expensive aspheric lenses. The combination of chip and package now becomes a low-cost solution that has manufacturing, marketing, and business advantages.

Figure 10

Light-versus-current characteristic for an uncoated 7-well laser. The slope efficiency is 0.4W/A at room temperature and the measured far field was 23° by 27°.

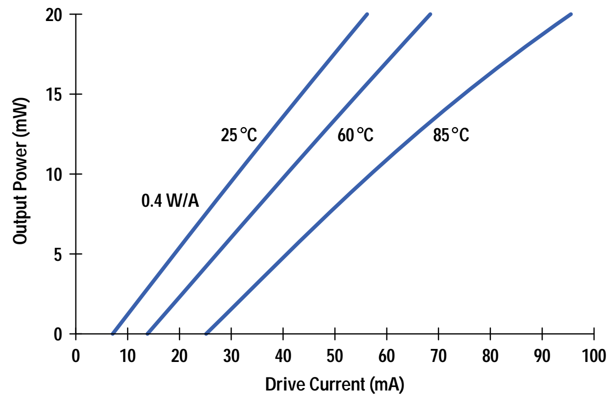

Uncooled 1300-nm Distributed Feedback Lasers

Uncooled distributed feedback lasers are emerging in the marketplace to replace cooled transmitters. The arena they address is the long-haul SDH/SONET specifications for 622 Mbits/s and 2.488 Gbits/s, where the dispersion and the window of operation cannot be achieved by a Fabry-Perot laser because of its broad spectral width and wavelength temperature coefficient. The principal difference between the Fabry-Perot laser and the distributed feedback laser is the addition of a grating layer in the device, which controls the fundamental operating wavelength. The difference in the characteristics of Fabry-Perot and distributed feedback lasers are highlighted in **Table I**.

Table I

Operating Characteristics of Fabry-Perot and Distributed Feedback Laser Diodes

Characteristic	Fabry-Perot	Distributed Feedback
Wavelength	Gain Peak	Bragg Mode
Wavelength Temperature Coefficient	0.3 to 0.5 nm/°C	<0.1 nm/°C
Spectral Width (rms)	1.7 to 2.5 nm	<1 nm at −20 dB
Side Mode Suppression	Multimode Operation	>30 dB

Distributed feedback lasers have some inherent problems achieving single-mode operation over the required operating temperature range of −40°C to +85°C. In the next sections, we will outline the main areas of concern and show how they can be tackled to produce a more manufacturable product.

Single-Mode Behavior

To gain insight into the basic principles of operation of distributed feedback lasers, we need to derive the coupled wave equations and then apply some approximations. This will highlight a significant problem found in conventional index-guided distributed feedback lasers, that is, single-mode yield (the percentage of devices that operate in one distributed feedback mode).

The introduction of a grating layer into the device structure produces a periodic variation in both the real and imaginary (gain) parts of the refractive index, which can be represented by the following equations:

$$n(z) = n_o + \Delta n \cos(2\beta z + \phi) \quad (4a)$$

$$\alpha(z) = \alpha_o + \Delta\alpha \cos(2\beta z + \phi), \quad (4b)$$

where n_o is the mean refractive index, α_o is the mean loss or gain, Δn and $\Delta\alpha$ are the perturbations from the mean, β is the propagation constant for the waveguide, and ϕ is a phase factor.

Substituting these into the wave equation and assuming a small perturbation of the traveling wave, that is, $\alpha \ll \beta$, $\Delta n \ll n$, and $\Delta\alpha \ll \alpha$, we obtain the following result for the propagation constant k of the perturbed wave:

$$k^2 = \beta^2 + 2j\beta\alpha_o + 4\beta[k_o\Delta n + j\Delta\alpha]\cos(2\beta z + \phi), \quad (5)$$

where k_o is the free-space propagation constant. The expression in brackets is defined as the real and imaginary parts of the grating coupling coefficient and is used to describe the interaction of the grating with the waveguide:

$$[k_o\Delta n + j\Delta\alpha] = \kappa = \kappa_r + j\kappa_i, \quad (6)$$

where κ is the complex coupling coefficient and defines the grating strength. On substitution of equation 5 back into the wave equation and assuming a trial solution of the E-field of the form:

$$E(z) = R(z)e^{-j\beta z} + S(z)e^{j\beta z}, \quad (7)$$

we arrive at the standard coupled mode representation to describe the forward S(z) and backward R(z) traveling waves in the cavity:

$$-dR/dz + (\alpha - j\delta)R = j\kappa S \quad (8a)$$

$$dS/dz + (\alpha - j\delta)S = j\kappa R. \quad (8b)$$

The new term δ is defined as the detuning of the main distributed feedback mode from the Bragg mode,* that is,

$$\delta = \beta - \beta_o = 2\pi n_{eff} L(\nu - \nu_o)/c,$$

where β is the propagation constant of a distributed feedback mode, β_o is the propagation constant of the Bragg or stop-band mode, n_{eff} is the effective refractive index, L is the cavity length, ν is the frequency, and c is the velocity of light. To simplify things further, we can neglect the influence of the facets by assuming perfect antireflective coatings. The traveling waves then become sinh functions in terms of the complex propagation constant γ:

$$R(z) = \pm \sinh\gamma(z + L/2) \quad (9a)$$

$$S(z) = \mp \sinh\gamma(z - L/2), \quad (9b)$$

where

$$\gamma^2 = (\alpha - j\delta)^2 - \kappa^2.$$

* The distributed feedback mode is the grating mode with the highest gain, the one that achieves lasing action first. The Bragg mode is the zeroth-order diffraction mode, defined by the pitch of the grating.

Substitution of $R(z)$ and $S(z)$ into equations 8a and 8b then produces the following general equations:

$$\gamma + (\alpha - j\delta) = j\kappa e^{\gamma L} \qquad (10a)$$

$$\gamma - (\alpha - j\delta) = j\kappa e^{-\gamma L}. \qquad (10b)$$

Invoking the high-gain approximation, that is, $\kappa \ll \alpha$, and inserting this into equation 10a, we obtain:

$$2(\alpha - j\delta) \approx \pm j\kappa \exp(\alpha - j\delta)L. \qquad (11)$$

The condition for the resonant modes of the cavity is found by taking the phase of this expression, which gives:

$$\delta L \approx (q + 1/2)\pi + \tan^{-1}(\kappa_i/\kappa_r), \qquad (12)$$

where q is the mode number. Thus, we obtain:

$$(\nu - \nu_o)(c/2n_{eff}L)^{-1} \approx q + 1/2 + (1/\pi)\tan^{-1}(\kappa_i/\kappa_r). \qquad (13)$$

Neglecting the facet reflectivity and facet phase contributions, the above expressions sum up the intrinsic problem with achieving single-mode operation in distributed feedback lasers. First, the resonances are approximately $c/2n_{eff}L$ apart, which is similar to the behavior of a Fabry-Perot resonator. Secondly, for the normal type of distributed feedback structure which uses predominantly index coupling (κ real), there is NO resonance at the Bragg mode. Instead, the condition is satisfied only for two degenerate modes on either side of the stop band. To achieve single-mode operation the phase condition should equal π when $q = 0$. This occurs for pure imaginary coupling when $\kappa_i > 0$ and $\kappa_r = 0$ or when a $\lambda/4$ phase shift is introduced into the grating.

Temperature Performance

The temperature performance of a distributed feedback laser is governed by several factors, including the detuning of the distributed feedback mode from the material gain peak, the strength of the grating, and the temperature performance of the active region. To achieve operation from −40°C to +85°C, we need to look at the fundamental picture of what happens to the laser gain spectrum and its relative strength and position with respect to the distributed feedback mode.

The SDH standards require a spectral purity corresponding to greater than 30 dB of side mode suppression, which requires a minimum modal gain difference of $\sim 5\ cm^{-1}$ between the dominant Fabry-Perot mode* and the distributed feedback mode. This is normally achieved by coating the facets of the distributed feedback laser to increase the mirror loss of the Fabry-Perot mode relative to the distributed feedback mode. We can understand this from the gain condition equation of a distributed feedback laser. The general gain condition for a distributed feedback laser is derived from the coupled mode equations by inserting the correct boundary conditions at the facets. We then obtain:

$$\frac{\left(r(\beta) - \sqrt{R_1}e^{j\phi_1}\right)\left(r(\beta) - \sqrt{R_2}e^{j\phi_2}\right)}{\left(1 - r(\beta)\sqrt{R_1}e^{j\phi_1}\right)\left(1 - r(\beta)\sqrt{R_2}e^{j\phi_2}\right)}\exp(\alpha L) = 1, \qquad (14)$$

where $r(\beta)$ is the grating reflectivity, which depends on propagation constant β, R_1 and R_2 are the facet reflectivities, ϕ_1 and ϕ_2 are the facet phases, α is the gain difference, and L is the cavity length. When $r(\beta) = 0$ we regain the Fabry-Perot laser round-trip gain condition as expected. Rearranging this into a more common form:

* Fabry-Perot modes are resonant cavity modes of the laser, i.e., $\lambda = 2m\pi/L$.

$$G = \alpha_i + \frac{1}{L}\ln\left[\frac{\left(1 - r(k)\sqrt{R_1}e^{j\phi_1}\right)\left(1 - r(k)\sqrt{R_2}e^{j\phi_2}\right)}{\left(r(k) - \sqrt{R_1}e^{j\phi_1}\right)\left(r(k) - \sqrt{R_2}e^{j\phi_2}\right)}\right], \quad (15)$$

where α_i is the internal absorption loss. We see that, essentially, the grating introduces an effective difference in the mirror loss between the distributed feedback mode and the Fabry-Perot mode that is a function of cavity length, facet reflectivity, facet phase, and grating coupling strength. This can now be used to estimate the gain difference between the Fabry-Perot mode and the distributed feedback mode (see **Figure 11**) as a function of the grating strength. To get a handle on the lower limit of grating strength to make the distributed feedback laser operate over the required temperature range we need to measure the modal gain spectrum for the various operating temperatures at fixed proportions of threshold and then compare this with mirror loss curves of the distributed feedback laser.

Figure 11

Calculated gain difference between the distributed feedback mode and the Fabry-Perot mode as a function of grating coupling coefficient κ. The Fabry-Perot mirror loss is 68 cm^{-1} and for a distributed feedback laser to work over the full temperature range a minimum κ of 60 cm^{-1} is required.

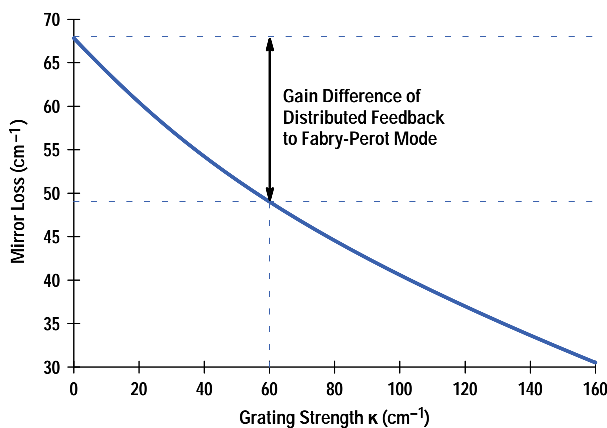

Figure 12

Measured gain spectra for a Fabry-Perot laser from −40°C to +85°C using the Hakki-Poali method. The three curves cross approximately 20 cm^{-1} from the gain equals loss condition (G=0) and 15 nm from the 25°C gain peak. This is used to estimate the minimum grating coupling strength required for full-temperature-range operation.

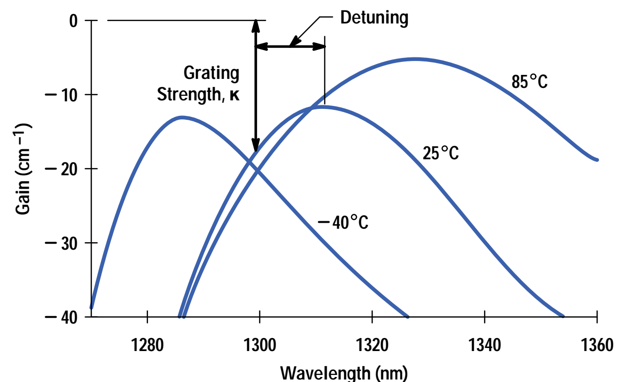

The modal gain of a 7-well 1300-nm Fabry-Perot laser was measured using the Hakki-Poali method[12] for three temperatures (see **Figure 12**). It shows that the three gain spectra cross at the short-wavelength side about 15 nm from the 25°C gain peak, and 20 cm^{-1} down from the gain equals loss condition (i.e., $G=0$). The curve closest to the gain condition is the 85°C spectrum which has a peak of −5 cm^{-1}, similar to the value needed for 30-dB side mode suppression. This indicates that for the distributed feedback mode to lase over this temperature range we have to impose a mirror loss difference of 20 cm^{-1}, which equates to a minimum grating coupling coefficient κ of 60 cm^{-1}. In conventional index-guided distributed feedback lasers the facet reflectivity and facet phase introduce some asymmetry in the gain of the two degenerate distributed feedback modes, producing single-mode devices. Previous analysis of the single-mode yield by many groups has shown that it drops off rapidly as the grating coupling strength increases, primarily because of the reduction in gain difference between the two stop-band modes as the facet contribution gets smaller.[13]

To overcome this problem we need to introduce some gain coupling to enhance the single-mode yield. The phase condition, equation 12, shows that there is a contribution of $\tan^{-1}(\kappa_i/\kappa_r)$. When κ_i is zero the phase condition implies that the distributed feedback laser has two modes, but the introduction of pure gain coupling, that is, $\kappa_i > 0$ and $\kappa_r = 0$, allows the

phase matching condition to be satisfied at the Bragg mode, which has the highest gain to propagate in the structure. Hence to achieve full-temperature-range operation of a distributed feedback laser, we must use a high coupling coefficient and introduce gain coupling to enhance the single-mode yield.

Device Results

The planar structure for the active region was based on our Fabry-Perot strained quantum well design. The grating was n^{++} doped to block the current periodically and thereby induce a current modulation in the active region. First-order gratings were defined by holography and dry etching. The devices were overgrown with approximately 300 nm of InP and then mesas were defined and wet chemically etched. Two further overgrowths were performed for realization of the standard current blocking structure. After metallization the chips were coated with either a combination of an antireflection coating and a high-reflection coating or only one facet was coated with an antireflection coating. The chips were tested from −40°C to +85°C in submodule packages with angle-ferrule connectors to minimize the optical return loss into the chip. The threshold current and spectra were characterized. The low threshold current achieved at 85°C was 26 mA for a full-temperature-range gain-coupled device (see **Figure 13**).

Figure 13

Light-current characteristic for a gain-coupled distributed feedback laser showing the excellent temperature characteristics that can be produced.

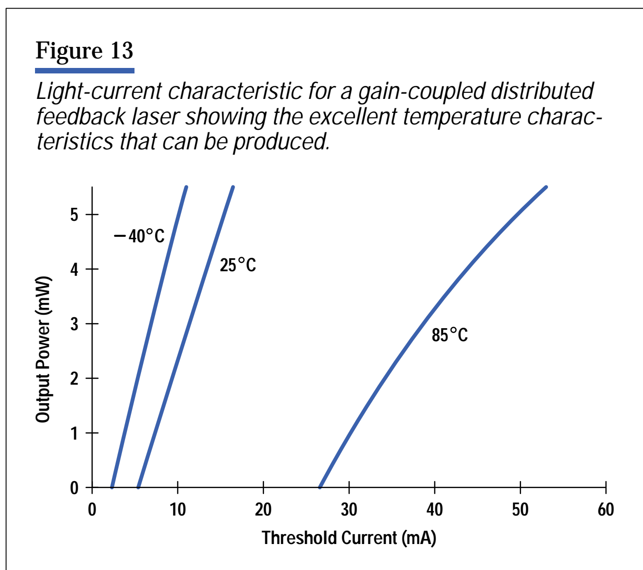

Figure 14

Wavelength temperature measurement of a positively detuned distributed feedback laser showing that the side mode suppression ratio drops below 30 dB at temperatures lower than −10°C and the laser becomes a Fabry-Perot laser at −40°C. This shows a limit on the positive detuning for successful low-temperature operation.

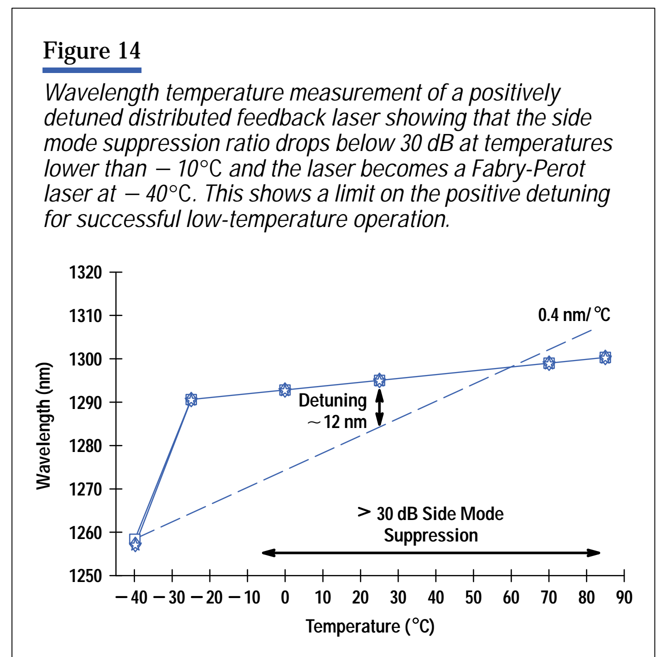

Investigation of the detuning of the distributed feedback mode with respect to the gain peak at 25°C showed that if the device was detuned to the longer-wavelength side by more than 10 to 15 nm, low-temperature operation was not achievable (see **Figure 14**), even though low threshold currents of only 18 mA could be achieved. Estimates from the detuning experiment revealed that effectively there was a 10-nm window for full-temperature-range operation with devices requiring 0-nm to −10-nm detuning to operate over the required range.

A major concern with distributed feedback lasers is the sensitivity to external reflections. Telecommunications distributed feedback lasers operating at 1550 nm normally employ an optical isolator in the package to prevent reflections that would perturb the optical signal. The main reason for this enhanced sensitivity compared to Fabry-Perot lasers is the antireflection coating on the front facet. With the antireflection coating, reflected light can easily perturb the internal optical field profile of the laser, causing either double-mode behavior, reduced side mode suppression, or noise on the data 1s (i.e., the on state).

To achieve low cost, the package should not use an optical isolator. Instead, we designed the grating structure to reduce the sensitivity. The SONET/SDH specifications require a transmitter device to operate with a maximum discrete reflectance of −25 dB and a maximum return loss of −20 dB from the optical plant or system. A mated connector should give around −40 dB return loss, while a connector to air gives −14 dB, a worst-case scenario. We varied the grating coupling strengths to calibrate the reflection sensitivity of our buried heterostructure distributed feedback lasers. The reflection sensitivity measurements showed that at relatively moderate grating strengths of 50 cm^{-1}, the distributed feedback spectrum was perturbed to optical return losses of more than −20 dB. For grating strengths (κ) of 90 cm^{-1} and 120 cm^{-1} the spectrum remained unperturbed even up to −14 dB optical return loss. This allowed us to gauge the minimum strength required in our design.

This need for high coupling coefficients for full-temperature-range operation and immunity to reflections is useful from a manufacturing standpoint because prohibitively expensive integral optical isolators are no longer required. The only problem that remains is the single-mode yield, which can be improved by the introduction of gain coupling.

Typically, the single-mode yield in our strained quantum well distributed feedback laser depends approximately on the number of wells in the structure. Extremly high single-mode yields of 70% to 80% have been achieved for 7-well devices with grating coupling coefficients (κL) of 2.5 to 3.5. These are extremly good results; typically, single-mode yields are much smaller than this at such high coupling coefficients. We observed a decrease in the yield as more quantum wells were introduced into the structure, with the single-mode yield being only 38% to 44% for 9-well structures for equivalent grating strengths. The final design required a trade-off between well number and single-mode yield to provide both good packaged temperature performance and high power.

Conclusion

We have discussed aspects of device design necessary to produce uncooled strained quantum well lasers for SONET/SDH/ATM systems. To cover long-haul, intermediate, and short-haul specifications, two distinct types of laser structure are required: distributed feedback and Fabry-Perot lasers. The short-haul and intermediate link applications can be covered by Fabry-Perot lasers which are simple to fabricate with a high manufacturing yield and are extremely reliable.

The long-haul market at 622 Mbits/s and 2.488 Gbits/s is addressed by our uncooled distributed feedback lasers. The basic difference is the mode selectivity introduced by the grating. The main problem for distributed feedback lasers is achieving operation over the temperature range of −40°C to +85°C. We showed how this can be done by the use of high grating coupling coefficients and gain coupling to increase the single-mode yield. The successful operation of our distributed feedback lasers from −40°C to +85°C with extremely good threshold and power characteristics shows these will play a key role in the successful deployment of FTTH and FTTC.

Acknowledgments

The authors would like to thank all the members of the device technology group at Ipswich for their support and hard work. Special thanks should be given to Herbert Lage for his contribution on the strained quantum well material growth and valuable discussions, to Paul Charles and Andrew McKee for the transition of the Fabry-Perot quantum well laser into production, to Ian Smith for all his hours working on characterization of the Fabry-Perot laser, and to Antony Hawkridge for reliability predictions and qualification data. Special thanks to Conrad Langton for the development of the semicircular high-speed buried heterostructure trenching process, which led to a reduction in stress effects, allowing the push forward to 2.488 Gbit/s operation. Finally, thanks to Richard Ash and Sean Amos for their support through both programs.

References

1. ITU-T Recommendation G.957, ITU-T Study Group XV, 1988-93.

2. A.R. Adams, “Band Structure Engineering for Low Threshold High Efficiency Semiconductor Lasers,” *Electronics Letters*, Vol. 22, 1986, pp. 249-250.

3. E. Yablonovich and E.O. Kane, “Reduction of the Lasing Threshold Current Density by Lowering the Valence Band Effective Mass,” *Journal of Lightwave Technology*, Vol. LT-4, May 1986, pp. 504-506.

4. J.W. Mathew and A.E. Blakeslee, “Defects in Epitaxial Multilayers,” *Journal of Crystal Growth*, Vol. 27, 1974, pp. 118-125.

5. P.J.A. Thijs, F.L. Tiemeijer, J.J.M. Binsma and T. van Dongen, “Progress in Long Wavelength Strained-Layer InGAs(P) Quantum Well Semiconductor Lasers and Amplifiers,” *IEEE Journal of Quantum Electronics*, Vol. 30, no. 2, 1994, pp. 477-499.

6. W.S. Ring, H. Lage, A.J. Taylor, I.S. Smith, and R. M. Ash, “Optimisation of highly efficient uncoated strained 1300nm InGaAsP MQW Lasers for uncooled high temperature operation,” paper ThG4, *Conference on Optical Fiber Communication, Technical Digest*, Vol. 2, 1996, p. 230.

7. V. Mikhaelashvili, N. Tessler, R. Nagar, G. Eisenstein, A.G. Dentai, S. Chandrasakhar, and C.H. Joyner, “Temperature Dependent Loss and Overflow Effects in Quantum Well Lasers,” *IEEE Photonics Technology Letters*, Vol. 6, no. 11, 1994, p. 1293.

8. C.E. Zah, R. Bhat, B.N. Pathak, F. Favire, W. Lin, M.C. Wang, N.C. Andreadakis, D.M. Hwang, M.A. Koza, T.P. Lee, Z. Wang, D. Darby, D. Flanders, and J.J. Hsieh, “High-Performance Uncooled 1.3-μm $Al_xGa_yIn_{1-x-y}As$/InP Strained Layer Quantum Well Lasers for Subscriber Loop Applications,” *IEEE Journal of Quantum Electronics*, Vol. 30, no. 2, 1994, pp. 511-523.

9. C.G. Van De Walle, “Band Line Ups and Deformation Potentials in the Model Solid Theory,” *Physical Review B*, Vol. 39, no. 3, 1989, pp. 1871-1883.

10. J.R. Biard, W.N. Carr, and B.S. Reed, “Analysis of a GaAs Laser,” *Transactions of the Metallurgical Society of the AIME*, Vol. 230, 1964, pp. 286-290.

11. J.I. Pankove, *IEEE Journal of Quantum Electronics*, Vol. QE-4, no. 4, 1968, p. 119.

12. B.W. Hakki and T.L. Poali, “Gain Spectra in GaAs Double Heterostructure Injection Lasers,” *Journal of Applied Physics*, Vol. 46, March 1975, pp. 1299-1306.

13. K. David, G. Morthier, P. Vankwikelberge, R.G. Baets, T. Wolf and B. Borchert, *IEEE Journal of Quantum Electronics*, Vol. QE-27, 1991, p. 1714.

William S. Ring

Bill Ring is a principal engineer and project leader with HP’s Ipswich, England Components Operation, responsible for development of 1300-nm strained quantum well and uncooled distributed feedback laser chips. He is an expert in III-V semiconductor laser theory and his 1992 PhD dissertation was on the efficiency of strained and unstrained light-emitting devices. Before joining HP in 1994 he was a research officer with Optronics Ireland.

Simon J. Wrathall

Simon Wrathall is a senior technician presently working on device characterization, test jigs, and test software at HP’s Ipswich, England Components Operation. He holds a BSc degree in physics and astrophysics and is a native of Ipswich.

Adrian J. Taylor

Adrian Taylor is a senior engineer in charge of the epitaxial growth area at HP’s Ipswich, England Components Operation. He holds an MSc degree in instrumentation and analytical science (1986) from the University of Manchester Institute of Science and Technology. Born in Redhill, Surrey, UK, he is married and has a daughter. Before joining HP he was with GEC for seven years.

▶ Go to Next Article

▶ Go to Journal Home Page